Available online at www.sciencedirect.com
ScienceDirect
Trans. Nonferrous Met. Soc. China 34(2024) 2900−2917
Transactions of Nonferrous Metals Society of China
www.tnmsc.cn

Influence of thermomechanical treatment on recrystallization and softening resistance of Cu−6.5Fe−0.3Mg alloy

Zhen-xia LIU[1], Da-wei YUAN[1], Xin LUO[2], Lan-hao WANG[2], Jin-shui CHEN[2], Hui-ming CHEN[1], Xiang-peng XIAO[1], Bin YANG[2]

1. College of Advanced Copper Industry, Jiangxi University of Science and Technology, Yingtan 335000, China;
2. Faculty of Materials Metallurgy and Chemistry, Jiangxi University of Science and Technology, Ganzhou 341000, China

Received 10 March 2023; accepted 13 October 2023

Abstract: The recrystallization and softening resistance of a Cu−6.5Fe−0.3Mg (mass fraction, %) alloy prepared by Process 1 (cold rolling heat treatment) and Process 2 (hot/cold rolling heat treatment) were studied using Vickers hardness tests, tensile tests, scanning electron microscopy and transmission electron microscopy. The softening temperature, hardness and tensile strength of the alloy prepared by Process 2 were 110 °C, HV 15 and 114 MPa higher, respectively, than those of the alloy prepared by Process 1 after aging at 300 °C. The recrystallization activation energy of the alloys prepared by Process 1 and Process 2 were 72.83 and 98.11 kJ/mol, respectively. The pinning effects of the precipitates of the two alloys on grain boundaries and dislocations were basically the same. The softening mechanism was mainly attributed to the loss of dislocation strengthening. The higher Fe fiber density inhibited the average free migration path of dislocations and grain boundary migration in the alloy, which was the main reason for higher softening temperature of the alloy prepared by Process 2.

Key words: Cu−6.5Fe−0.3Mg alloy; hot rolling; recrystallization activation energy; softening mechanism; dislocation strengthening

1 Introduction

Cu−Fe alloys are hard, electrically conductive, and have remarkably soft magnetic properties. They are widely used in heat sinks, optical devices, mobile phone sockets, electrical contacts, and shielding materials [1−3]. With the development of industrial technology and the advent of the 5G era, there has been a trend towards the development of high-current large-capacity batteries, electronic materials, and mobile phone wireless base stations. Large currents inevitably generate more heat. Consequently, there is greater demand for thermally conductive, heat-resistant materials. In addition, the stability of electrical contacts is crucial for the stable operation of plug-ins. Therefore, the high-temperature softening resistance of the Cu−Fe alloy materials is particularly important.

Cu−Fe alloy has a higher interface volume ratio and higher energy at the phase interface, which increases the driving force for the recrystallization of the alloy [4], thereby reducing high temperature softening resistance of the alloy. The combination of large plastic deformation and multi-stage heat treatment is necessary for the improvement of the mechanical and electrical properties of Cu−Fe alloys [1]. The Fe phases are

Corresponding author: Da-wei YUAN, Tel: +86-18270720422, E-mail: yuan_dw@126.com;
Bin YANG, Tel: +86-13970798000, E-mail: yangbin@jxust.edu.cn
DOI: 10.1016/S1003-6326(24)66584-2

fibrous, and the density of defects such as dislocations and vacancies in the Cu increases significantly during plastic deformation, which is the main reason for the improvement of the mechanical properties of the alloy [5−7]. However, the large deformation energy storage increases the recrystallization nucleation driving force and grain boundary mobility of the alloy, and the fine Fe fibers are prone to fracture and spheroidize during the heat treatment process. This results in a decrease in the high-temperature softening resistance of the Cu−Fe alloy [8]. Previous studies have shown that alloying with elements such as Cr [9,10], Mg [11,12], and Zr [13,14] can significantly improve the high-temperature softening resistance of Cu alloys. The elemental Cr mainly dissolves in the Fe phase. This inhibits grain boundary diffusion and recrystallization, thereby improving the heat resistance of the Fe fibers and the softening temperature of the Cu−Fe alloys [10]. GUO et al [13] found that elemental Zr effectively improved the thermal stability of a Cu−10Fe−1.5Ag alloy by up to approximately 50 °C. The main reason for this was that the Zr in the Cu alloy took the form of a diffusion compound, which hindered the diffusion and recrystallization of the Cu matrix grain boundaries and improved the softening temperature of the alloy. YUAN et al [12] found that the elemental Mg is enriched at the Cu/Fe phase interface, thereby inhibiting the recrystallization of the Cu matrix and enhancing the heat resistance of the Fe fibers. The alloying elements Cr, Mg, and Zr can improve the softening temperature of Cu−Fe alloys, but the effect is not obvious.

The density and distribution of Fe fibers are crucial for the high-temperature softening resistance of Cu−Fe alloys. SARKAR et al [15] synthesized the hierarchical fiber microstructures by rapid solidification and produced Cu−Fe−Si alloys with good thermal stability. In addition, thermo-mechanical treatment can significantly increase the density of Fe phase particles and optimize its distribution. ZHANG et al [16] investigated fracture behavior between the dendrite arms of the primary Fe phases during cold working. This increased the density of the Fe phase particles and the tensile strength of the alloy. However, the mechanism by which thermomechanical treatment influences the high-temperature softening resistance of a Cu−Fe alloy has not yet been reported.

Based on the analyses described above, in the present study, two preparation processes, i.e., Process 1 (cold rolling heat treatment) and Process 2 (hot/cold rolling heat treatment), were designed to explore the influence of thermomechanical treatment on the mechanical properties and softening temperature of a Cu−6.5Fe−0.3Mg (mass fraction,%) alloy. The mechanism by which Fe fibers influence alloy recrystallization and grain coarsening behavior was also elucidated.

2 Experimental

The two preparation processes were designed for the alloy after homogenization at 950 °C for 2 h, and a schematic diagram illustrating the processes is shown in Fig. 1. The hot rolling temperature was 950 °C and the compression ratio was 82%. The compression ratios of the two cold rolling processes

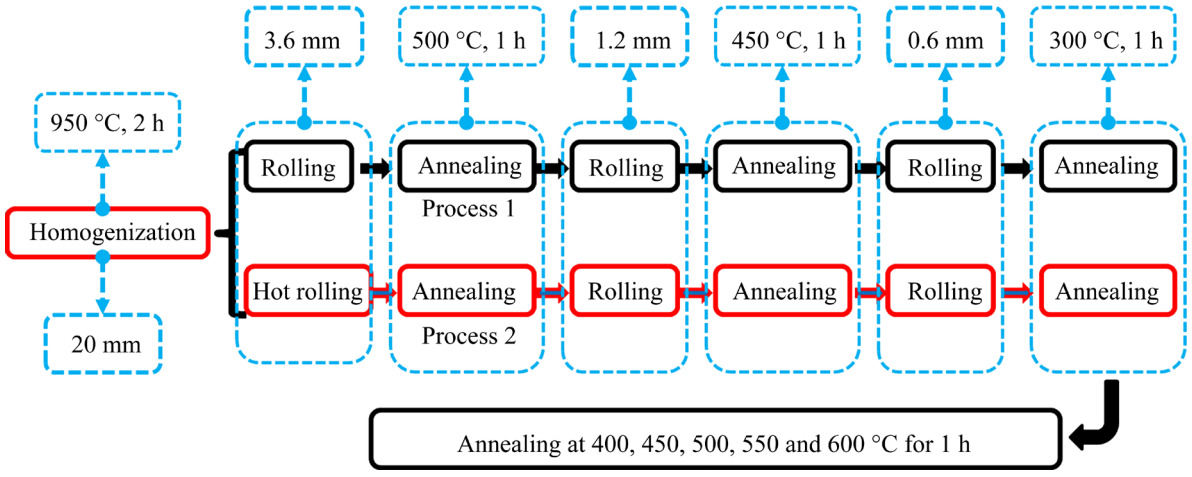

Fig. 1 Processing routes of Cu−6.5Fe−0.3Mg alloys

were 66.7% (3.6−1.2 mm) and 50% (1.2−0.6 mm), respectively. The plastic deformation in Process 1 was due to cold rolling. The first plastic deformation in Process 2 was due to hot rolling, and the second and third plastic deformation processes were due to cold rolling. Two intermediate annealing processes, i.e., at 500 and 450 °C for 1 h, were designed for Processes 1 and 2. Consequently, internal stress was eliminated from the alloy, and its plastic deformation behavior was improved. Furthermore, the processes avoided the fracture and spheroidization of the Fe fibers. Aging treatments at various temperatures were designed to determine the optimal performance of the alloy. Samples with peak hardness after aging at 300 °C for 1 h were selected for annealing at 400, 450, 500, 550, and 600 °C for 1 h to investigate the recrystallization behaviors and softening temperatures of the alloys prepared using Processes 1 and 2.

The hardness and strength of each alloy were tested using a QX.20-05 universal tensile testing machine and a SHYCHVT−5Z Vickers hardness tester (Laizhou Huayin). The yield strength was determined three times and the hardness was determined eight times. The average test point spacing and thermal drift correction values were 25 μm and 0.05 nm/s, respectively. The evolution of the microstructure of each sample was revealed by optical microscopy (OM; Axiolab 5, Zeiss, Germany), scanning electron microscopy (SEM; Mira3 LMH, TESCAN), electron backscattered diffraction (EBSD), and transmission electron microscopy (TEM; TecnaiG2-20, FEI) at 200 kV. The SEM acceleration voltage was 20 kV. The EBSD samples were fabricated by grinding, polishing, electrolytic double-jetting, and ion thinning. The accelerating voltage, grating value, and scan step size were 20 kV, 120, and 0.3 μm, respectively.

3 Results

3.1 Microstructure

Figure 2 shows the OM microstructures and element line scan analysis results of the homogenized alloys. It was clear that the addition of Mg optimized the distribution of the primary Fe phase and refined the Cu grains. There were numerous fine Fe phases in the Cu−6.5Fe−0.3Mg alloy, mainly distributed at the grain boundaries, which may promote non-uniform nucleation of the alloy and refine the Cu grains. The addition of Mg promoted the nucleation and precipitation of the Fe phase at the grain boundaries, which had the effect of pinning dislocations and inhibiting the diffusion of the grain boundaries [6,7]. Furthermore, Fig. 2(c) indicated that there was a greater distribution of elemental Mg around the spherical Fe phase than in the other regions.

Figure 3 shows the SEM images of the Cu−6.5Fe−0.3Mg alloys. Figures 3(a1, b1), (a2, b2), and (a3, b3) are the SEM images after rolling at a ratio of 97%, aging at 300 °C, and annealing at 550 °C,

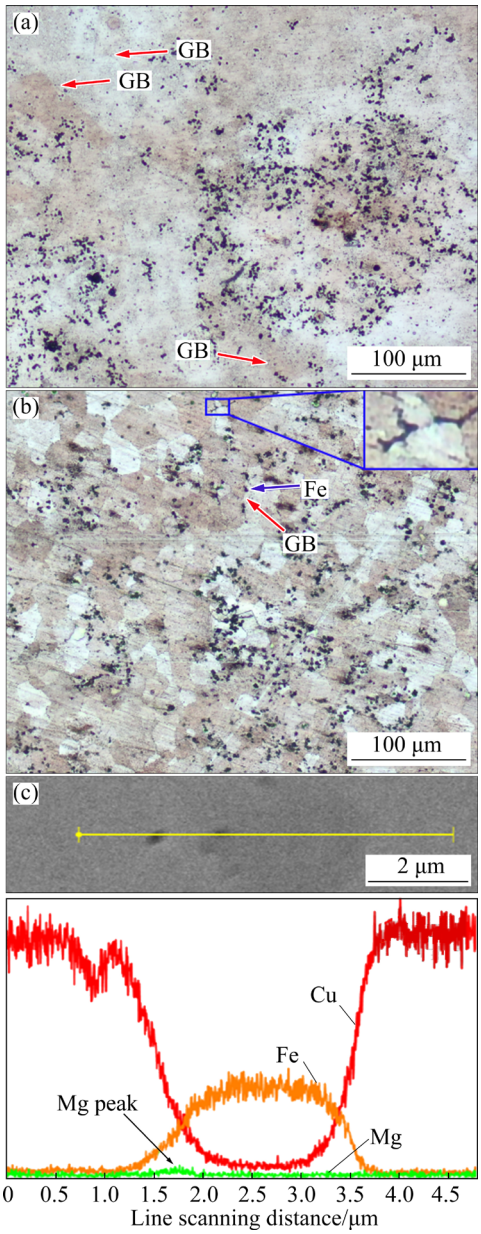

Fig. 2 OM images (a, b) and element line scan analysis results (c) of homogenized alloys: (a) Cu−6.5Fe; (b, c) Cu−6.5Fe−0.3Mg

respectively. The spherical Fe phases underwent plastic deformation during large plastic deformation to form fibrous Fe phases. However, the Fe fibers in the alloy prepared by Process 2 were longer, denser, and more uniformly distributed. This may be attributed to the smaller deformation resistance of the fine Fe phases. The average Fe fibers spacing of the alloy prepared by Process 2 was 3.5 μm, which was 1.3 μm smaller than that of the alloy prepared by Process 1. In addition, there was no significant change in the Fe fiber morphology after aging and annealing, although the density of the Fe fibers in the alloy prepared using Process 2 was always greater than that in the alloy prepared using Process 1.

Figure 4 shows the EBSD microstructures of

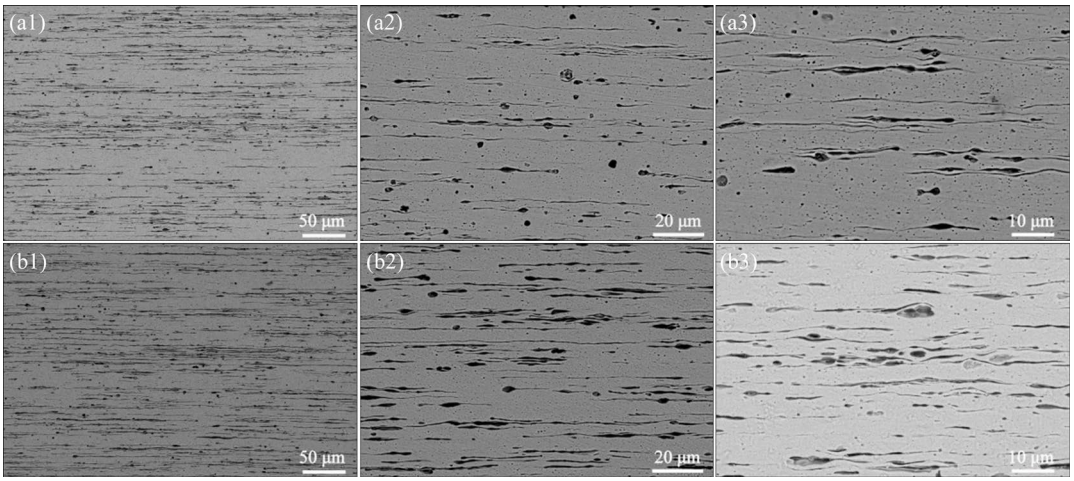

Fig. 3 SEM images of Cu−6.5Fe−0.3Mg alloys prepared by Process 1 (a1−a3) and Process 2 (b1−b3): (a1, b1) 97% rolling; (a2, b2) Aging at 300 °C; (a3, b3) Annealing at 550 °C

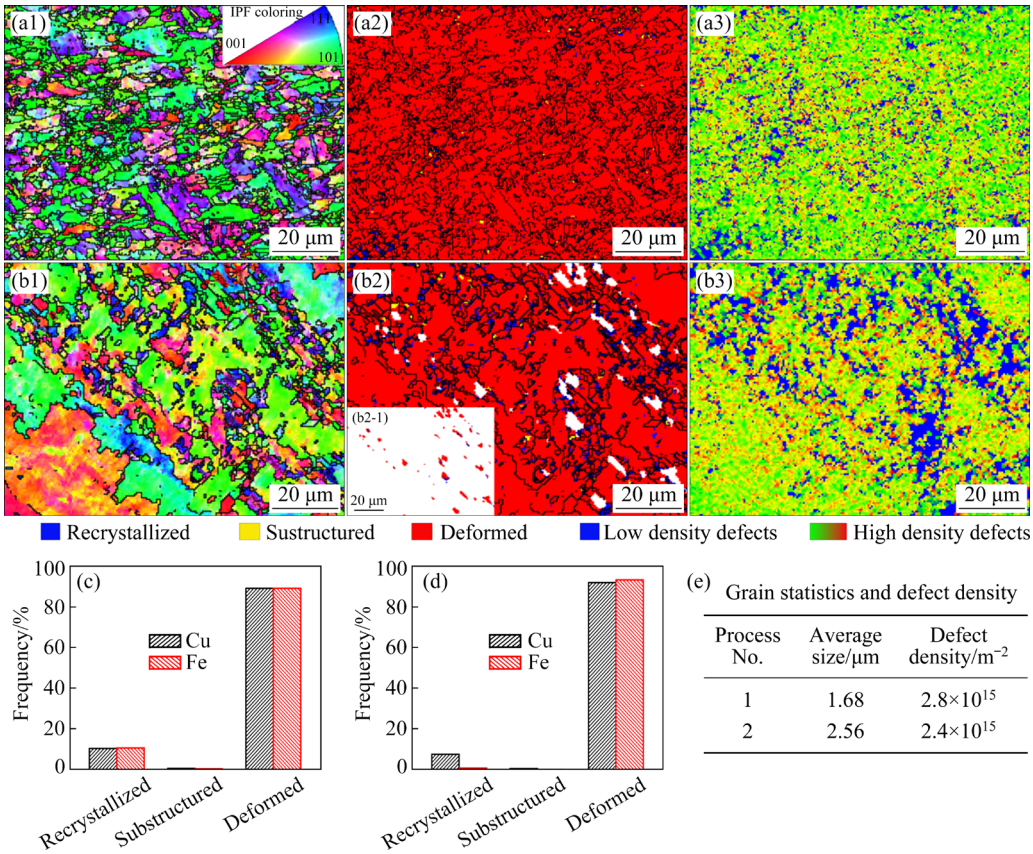

(e) Grain statistics and defect density

Process No.	Average size/μm	Defect density/m^{-2}
1	1.68	2.8×10^{15}
2	2.56	2.4×10^{15}

Fig. 4 EBSD microstructures (a1−a3, b1−b3), distribution of recrystallization (c, d), and grain statistics and defect density (e) of Cu−6.5Fe−0.3Mg alloys after aging at 300 °C for 1 h: (a1−a3, c) Process 1; (b1−b3, d) Process 2

the Cu−6.5Fe−0.3Mg alloys after aging at 300 °C for 1 h. Figures 4(a1−a3) show the microstructure of the alloy prepared by Process 1. The grains with low-angle grain boundaries (adjacent grains with a phase difference of less than 10°) were arranged in rod shapes along the deformation direction, and the alloy basically retained its deformed microstructure (Fig. 4(a2)). Figures 4(b1−b3) show the microstructure of the alloy prepared by Process 2. The grains with low-angle grain boundaries and Fe phases were distributed in long strips in the alloy. Similar to the alloy prepared using Process 1, the alloy retained its deformed microstructure (Fig. 4(b2)). However, the grains of the alloy prepared using Process 2 were longer than those of the alloy prepared using Process 1.

The dislocations in the alloys prepared using the two processes increased rapidly owing to slippage and climbing. Numerous vacancies and dislocations were formed during the deformation process, resulting in an increase in the alloy defect density (the total number of defects such as dislocations, vacancies per unit area, and low-angle grain boundaries), as shown in Figs. 4(a3) and (b3). This was consistent with previous reports [6,7]. An increase in the number of defects provides favorable conditions for recrystallization nucleation and atomic diffusion. The defect density (ρ) of an alloy can be calculated using the formula: $\rho=2\sqrt{3}\theta/(3bh)$, where θ, b, and h are the average orientation difference, the amplitude of Burgers vector, and the step size (0.3 μm), respectively. The defect density of the alloy prepared using Process 1 (2.8×10^{15} m^{-2}) was larger than that of the alloy prepared using Process 2 (2.4×10^{15} m^{-2}), as shown in Fig. 4(e). The figure shows that the alloy prepared using Process 1 was easier to nucleate and recrystallize in a high-temperature environment.

Figure 5 shows the EBSD microstructures of the Cu−6.5Fe−0.3Mg alloys after annealing at 450 °C for 1 h. The Cu grain boundary of the alloy prepared using Process 1 changed from low-angle to high-angle, mainly owing to the recrystallization behavior of the alloy, and the recrystallization proportion of the alloy reached almost 60%. In contrast, the alloy prepared using Process 2 retained a small-angle grain boundary, and its recrystallization proportion was only 12.3%, which was far lower than that of the alloy prepared by Process 1. This demonstrates that the alloy prepared using Process 2 had higher recrystallization and softening temperatures. In addition, the Fe phases in the alloys prepared by the two processes basically retained a variable morphology.

Figure 6 shows the EBSD microstructures of the Cu−6.5Fe−0.3Mg alloys after annealing at 550 °C for 1 h. Figures 6(a1−a3) show the microstructure of the alloy prepared by Process 1. There were numerous recrystallized grains with high-angle grain boundaries (adjacent grains with a phase

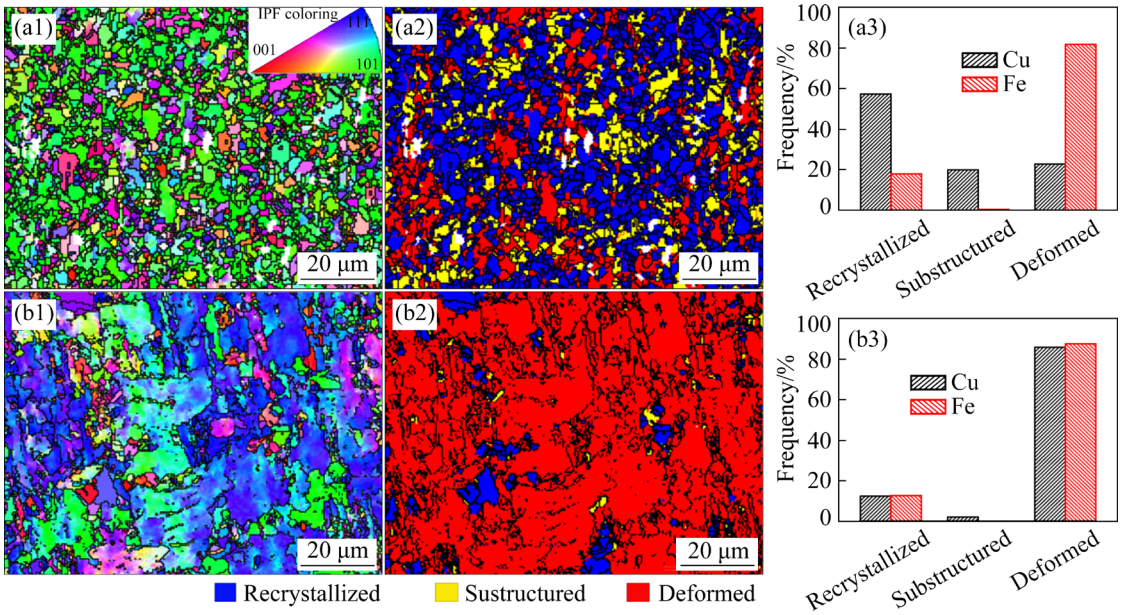

Fig. 5 EBSD microstructures (a1, a2, b1, b2) and frequency of recrystallization (a3, b3) of Cu−6.5Fe−0.3Mg alloys after annealing at 450 °C for 1 h: (a1−a3) Process 1; (b1−b3) Process 2

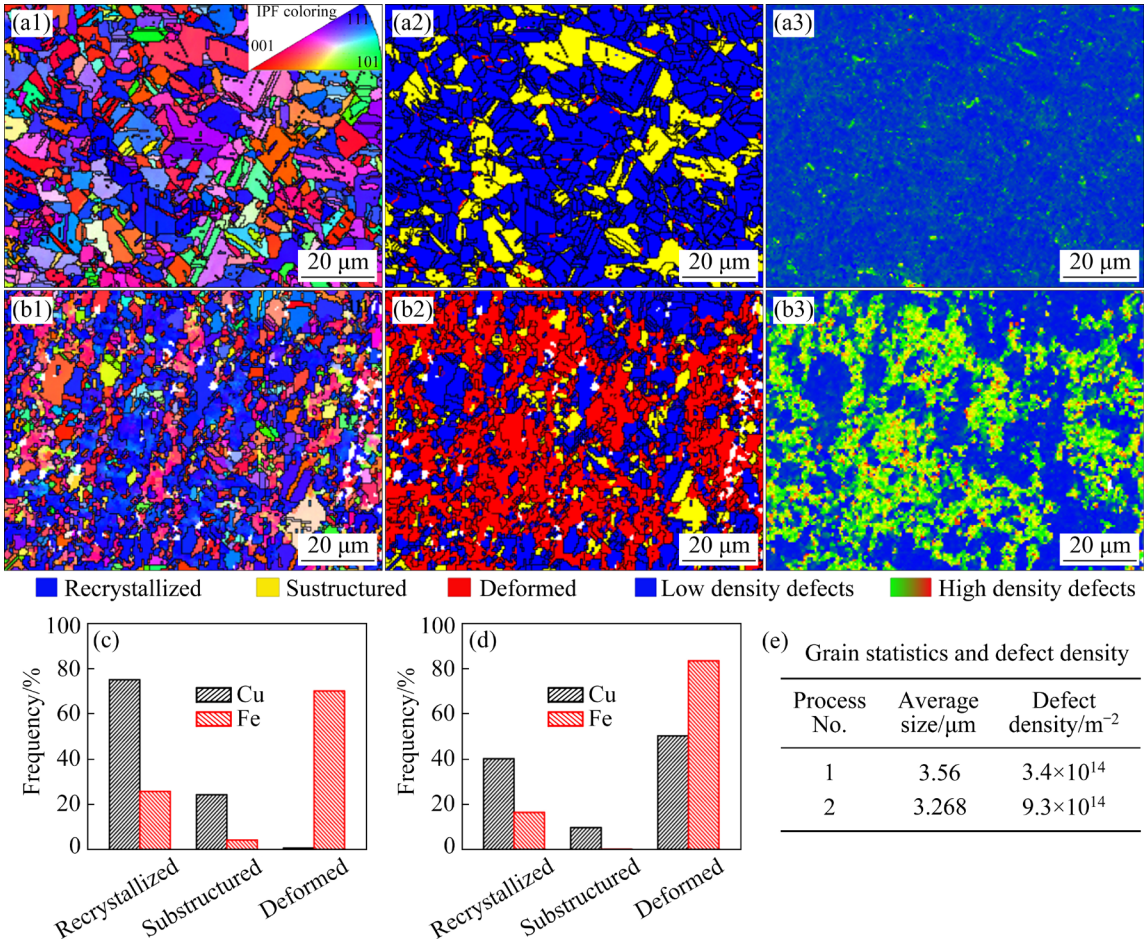

(e) Grain statistics and defect density

Process No.	Average size/μm	Defect density/m^{-2}
1	3.56	3.4×10^{14}
2	3.268	9.3×10^{14}

Fig. 6 EBSD microstructures (a1−a3, b1−b3), frequency of recrystallization (c, d), and grain statistics and defect density (e) of Cu−6.5Fe−0.3Mg alloys after annealing at 550 °C for 1 h: (a1−a3, c) Process 1; (b1−b3, d) Process 2

difference greater than 10°) and annealing twins. The alloy basically recovered and recrystallized. Figures 6(b1−b3) show the microstructure of the alloy prepared using Process 2. It is obvious that numerous grains retained low-angle grain boundaries, and that the matrix still had a deformed microstructure. Therefore, the results did not differ significantly from those shown in Fig. 4(b2). The proportions of the recrystallized microstructures of Cu and Fe in the alloy prepared using Process 2 were 40.1% and 12.6%, respectively, which were 35% and 13.4% smaller than those in the alloy prepared using Process 1 (Figs. 6(c) and (d)). In general, the alloys formed undistorted grains by nucleation and growth through recrystallization. Therefore, the defects of the alloys were greatly reduced as recrystallization progressed (Figs. 6(a2, a3, b2, b3)). It is worth noting that the alloy prepared using Process 2 still retains a higher defect density compared to the alloy prepared using Process 1 (Fig. 6(e)). This may be attributed to the dense Fe fibers, which suppressed the annihilation of dislocations and vacancies. The grain sizes of the alloys prepared using the two processes did not differ significantly.

Figure 7 shows the XRD results of the aged and annealed Cu−6.5Fe−0.3Mg alloys. The crystal plane indices of the Cu and Fe phases in the alloys prepared using the two processes were the same. The indices of the Cu phases were mainly (111), (200), (220), (311), and (222), and those of the α-Fe phases were mainly (110), (200), and (211). It is worth noting that all the Cu peaks of the alloys prepared using the two processes shifted to the right after annealing at 450 °C, but the shift angles of the peaks were not exactly the same. The precipitation of solid solution atoms leads to the migration of all Cu peaks. Moreover, a decrease in the density of defects such as dislocations and vacancies leads to a decrease in the degree of lattice distortion, which causes individual peak shifts [9]. Compared with the 97% rolled alloy, the peak maximum shift angle

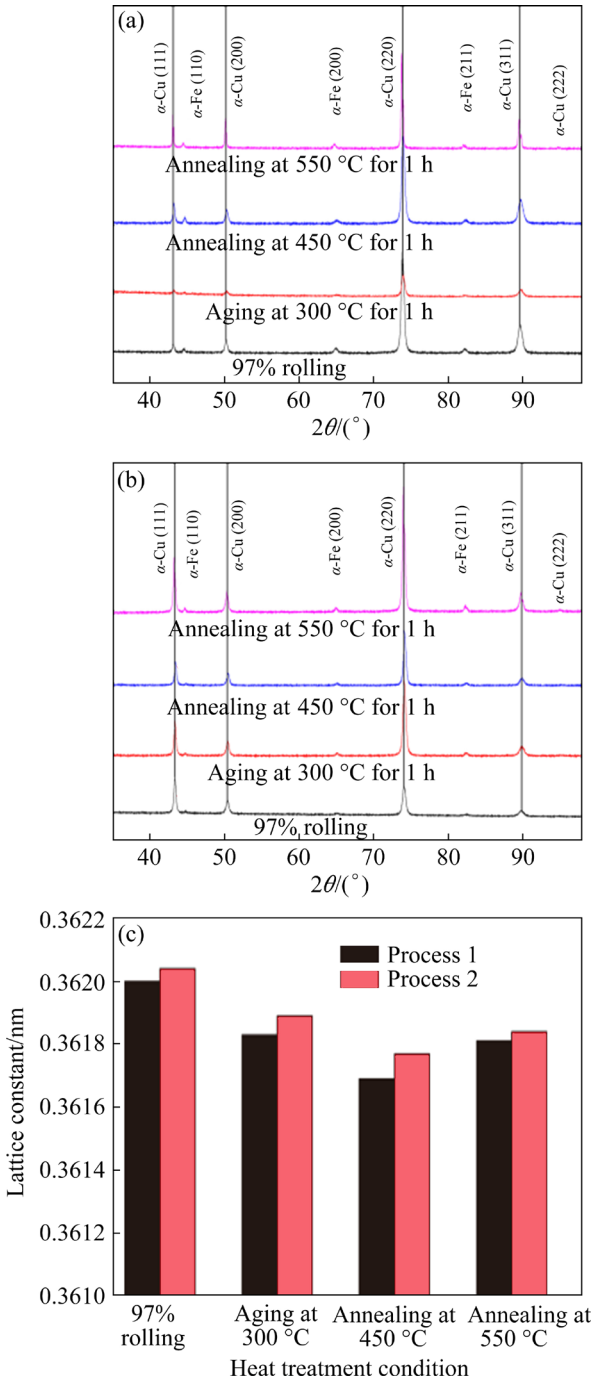

Fig. 7 XRD patterns (a, b) and lattice constants (c) of Cu−6.5Fe−0.3Mg alloys: (a) Process 1; (b) Process 2

of the alloy prepared using Process 2 was 0.15°, whereas the peak maximum shift angle of the alloy prepared using Process 1 was 0.18°. This shows that the dislocation density of the alloy prepared using Process 1 decreased more, which reflects the greater degree of recrystallization. As the annealing temperature increased to 550 °C, the Cu peaks in the alloys prepared using the two processes shifted slightly to the right. This may be attributed to the redissolution of the Fe phase at high temperatures, which is consistent with previous studies [17].

The lattice constants of the alloys prepared using the two processes first decreased and then increased slightly as the annealing temperature was increased. It is worth noting that the difference between the lattice constants of the two alloys gradually increased. This further indicates that the alloy prepared using Process 2 had a lower degree of recrystallization.

The TEM microstructure was examined to further investigate the microstructure of the 97% deformed Cu−6.5Fe−0.3Mg alloy, and the results are shown in Fig. 8. The selected area diffraction pattern (SADP) is shown in Fig. 8(c). Analysis of the SADP reveals that the elongated second phase of the alloy was $[011]_{\alpha\text{-Fe}}$. It is obvious that the elongated Cu grains and Fe fibers were arranged alternately in the alloys prepared using the two processes, although they were more densely arranged in the alloy prepared using Process 2.

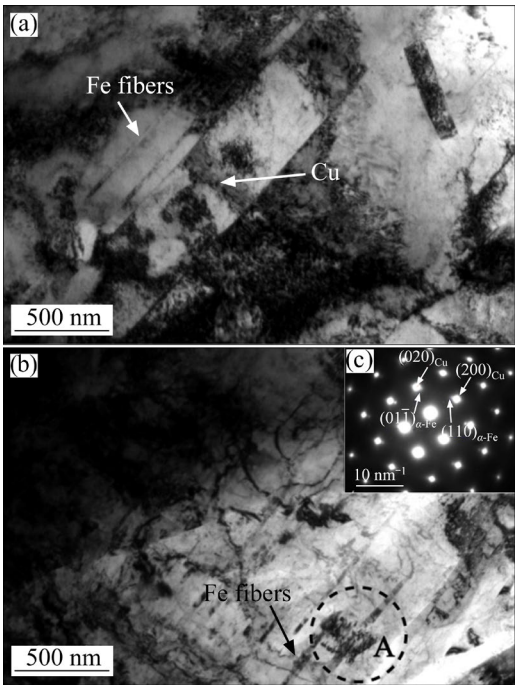

Fig. 8 TEM images of Cu−6.5Fe−0.3Mg alloys after 97% rolling: (a) Process 1; (b) Process 2; (c) Selected area diffraction pattern

Figure 9 shows the TEM microstructures of the Cu−6.5Fe−0.3Mg alloys after aging at 300 °C. The alloys prepared using the two processes retained numerous dislocations, but there were a small number of subgrains in the alloy prepared

using Process 1, indicating that the recovery microstructure already existed in the alloy. In addition, there were numerous nano-precipitated Fe phases with spherical or rod-shaped particles in the alloys prepared by the two processes. The average diameter of the precipitates in the alloy prepared using Process 2 was 6.81 nm, which was 0.4 nm smaller than that of the alloy prepared using Process 1.

Figure 10 shows the TEM surface scan results of the alloy prepared using Process 1 after aging at 300 °C for 1 h. The second phase in the alloy during the annealing or aging processes was the precipitated Fe phase. It is worth noting that, compared with the Cu matrix, more elemental Mg was distributed at the Cu/Fe phase interface (Fig. 10(d)), which was consistent with the results from a previous report [12]. This can inhibit the coarsening of the Fe phase.

To investigate the recrystallization behavior of the alloys prepared using the two processes, the alloys aged at 300 °C were subjected to isochronous annealing treatment for 1 h. Figure 11 shows the TEM microstructures of the Cu−6.5Fe−0.3Mg alloys after annealing at 450 °C for 1 h. There were numerous recrystallized grains and annealing twins in the Cu−6.5Fe−0.3Mg alloy prepared using Process 1, and the dislocation content was greatly reduced. However, numerous dislocations remained in the Cu−6.5Fe−0.3Mg alloy prepared using Process 2, and no recrystallized grains were found, indicating greater resistance to recrystallization.

Figure 12 shows the TEM microstructures of the Cu−6.5Fe−0.3Mg alloys after annealing at 550 °C for 1 h. It is obvious that the recrystallized grains of the alloy prepared using Process 1 were abnormally coarsened after annealing at 550 °C for 1 h. Numerous substructure microstructures and fine recrystallized grains were found in the alloy prepared using Process 2. The fine Fe fibers in the

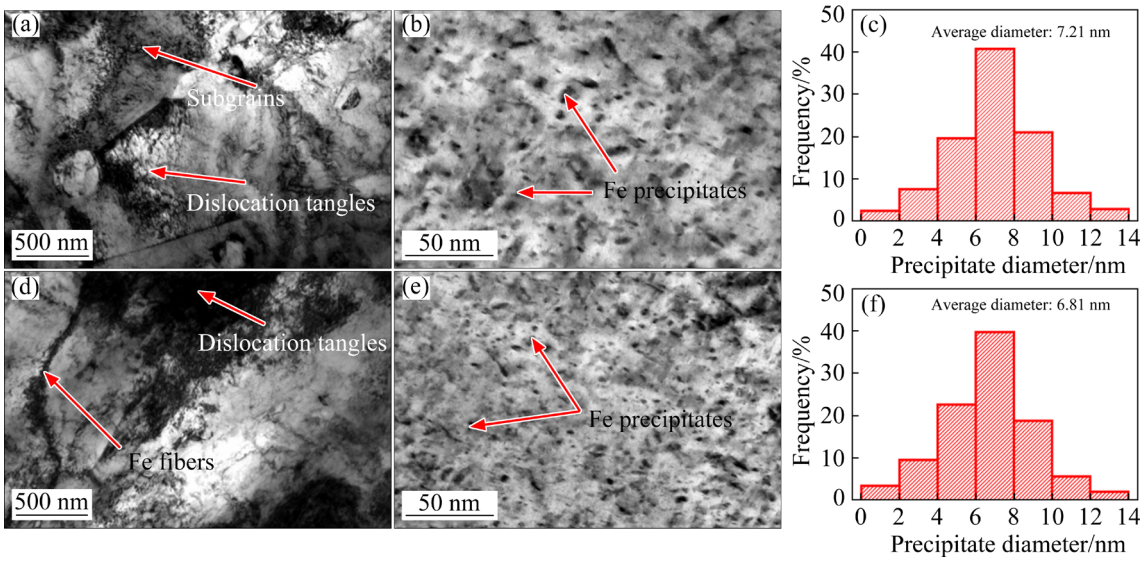

Fig. 9 TEM images (a, b, d, e) and precipitate size distribution (c, f) of Cu−6.5Fe−0.3Mg alloys after aging at 300 °C for 1 h: (a−c) Process 1; (d−f) Process 2

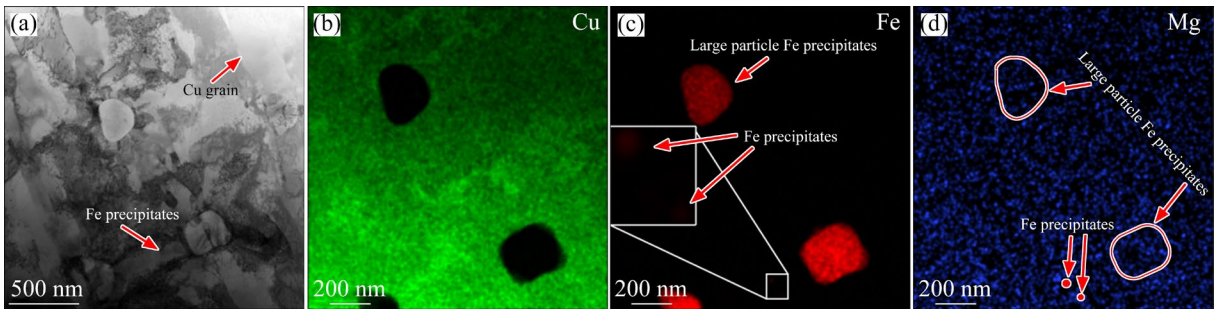

Fig. 10 TEM image (a) and EDS mappings (b−d) of Cu−6.5Fe−0.3Mg alloy prepared by Process 1 after aging at 300 °C for 1 h

alloy prepared using Process 2 were fractured and spheroidized. This reduced the inhibition effect of the Fe fibers on grain boundary migration and grain coarsening. However, some Fe fibers remained in the alloy prepared using Process 2. Furthermore, the precipitates in the two alloys were coarsened. This is not conducive to the pinning effect on the grain boundary. The average size of the precipitates in the alloy prepared using Process 2 was 7.65 nm, which was finer than that in the alloy prepared using process 1 (7.82 nm). The point scan results corresponding to EDS1 and EDS2 in Fig. 12 are shown in Fig. 13. The figure reveals that the nano-precipitated phases were Fe phases, and a small number of Fe atoms remained dissolved in the Cu matrix.

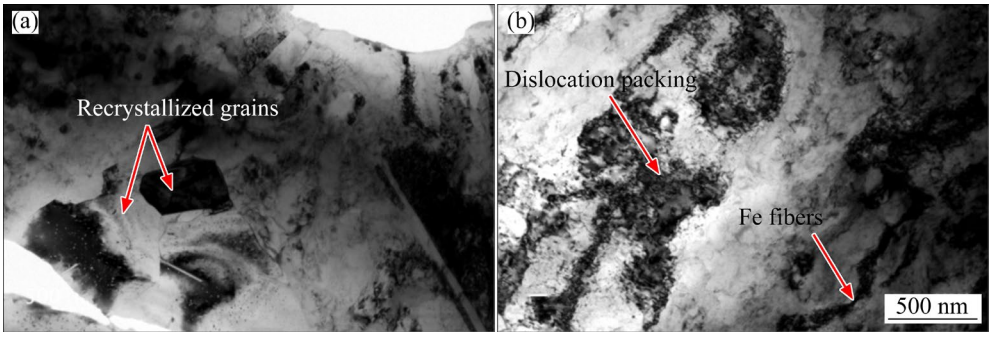

Fig. 11 TEM images of Cu−6.5Fe−0.3Mg alloys after annealing at 450 °C for 1 h: (a) Process 1; (b) Process 2

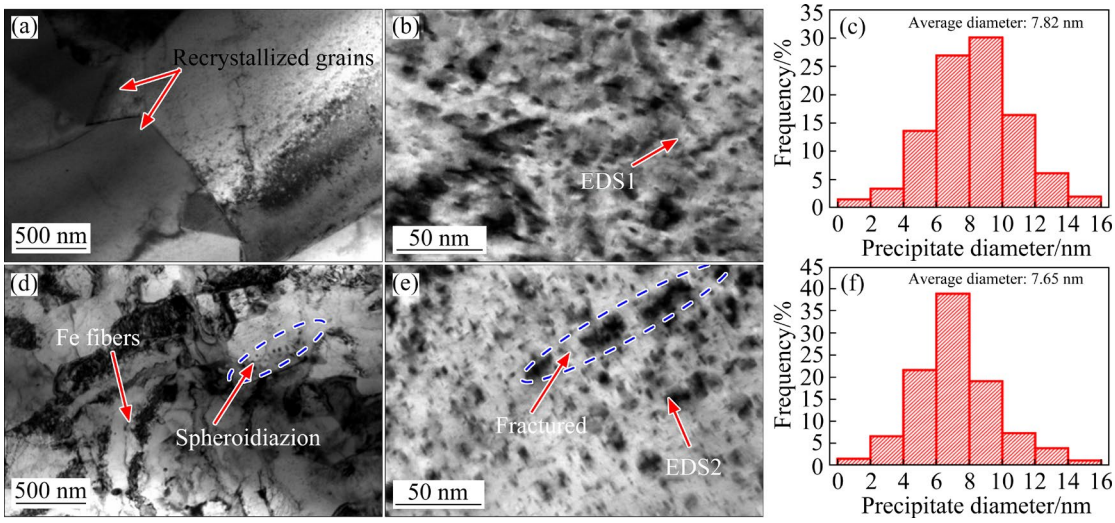

Fig. 12 TEM microstructures images (a, b, d, e) and precipitate size distribution (c, f) of Cu−6.5Fe−0.3Mg alloys after annealing at 550 °C for 1 h: (a−c) Process 1; (d−f) Process 2

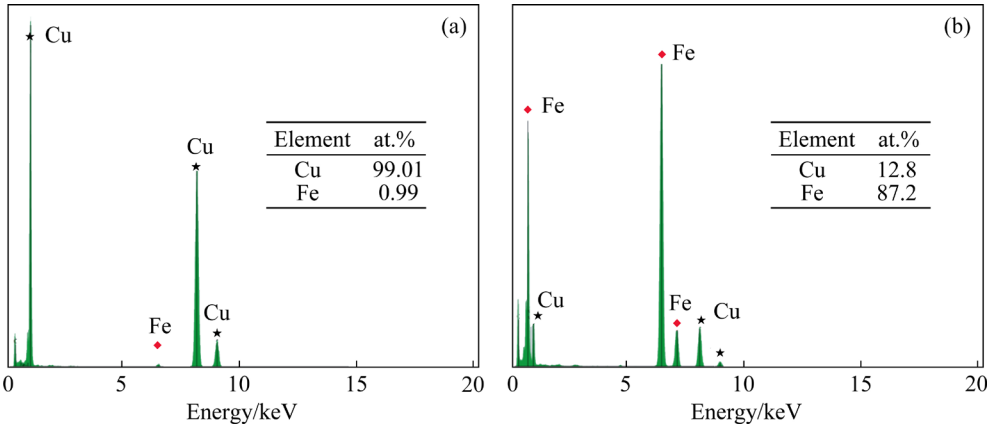

Fig. 13 Point scan results corresponding to EDS1 (a) and EDS2 (b) in Fig. 12

3.2 Mechanical properties

Figure 14 shows the Vickers hardness of the Cu−6.5Fe−0.3Mg alloys after aging. The Vickers hardness of the alloys prepared using the two processes increased at first and then decreased as the aging temperature increased, reaching a peak at 300 °C. At that point, the Vickers hardness of the alloy prepared using Process 2 was HV 207.7, which was HV 15 higher than that of the alloy prepared using Process 1.

To explore the softening behavior and conductivity of the Cu−6.5Fe−0.3Mg alloys prepared using the two processes, the alloys aged at 300 °C were subjected to isochronous annealing treatment. Figures 15(a, d) show the Vickers hardness and yield strength of the Cu−6.5Fe−0.3Mg alloy after isochronous annealing for 1 h, respectively. The Vickers hardness and yield strength values of the alloys prepared using the two processes decreased as the annealing temperature increased. However, the plastic properties of the alloys prepared using Processes 1 and 2 were improved and their tensile strengths were 704 and 818 MPa, respectively (Fig. 15(f)). The Vickers hardness and yield strength of the alloy prepared using Process 2 declined at a lower rate and to less extent than those prepared using Process 1. The Vickers hardness and yield strength values of the alloy prepared using Process 2 were reduced by HV 48 and 160 MPa, respectively, after annealing at 600 °C. These reductions were HV 15.7 and 90 MPa lower than those of the alloy prepared using Process 1.

Figures 15(b) and (e) show the percentages of hardness and yield strength, respectively. According to Standard GB/T 33370 — 2016, the softening temperature is that at which the hardness of the alloy drops to 80% of its initial value during heat treatment. The hardness percentage is proportional to the softening temperature: the faster the hardness percentage decreases, the lower the softening temperature of the alloy is. It is obvious from Fig. 15(b) that the Cu−6.5Fe−0.3Mg alloy prepared

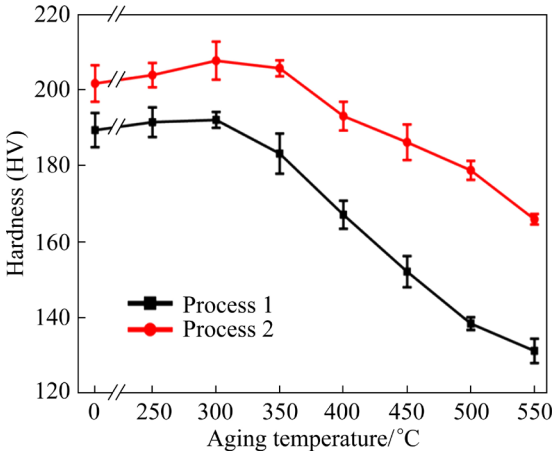

Fig. 14 Vickers hardness of Cu−6.5Fe−0.3Mg alloys after 97% rolling and aging

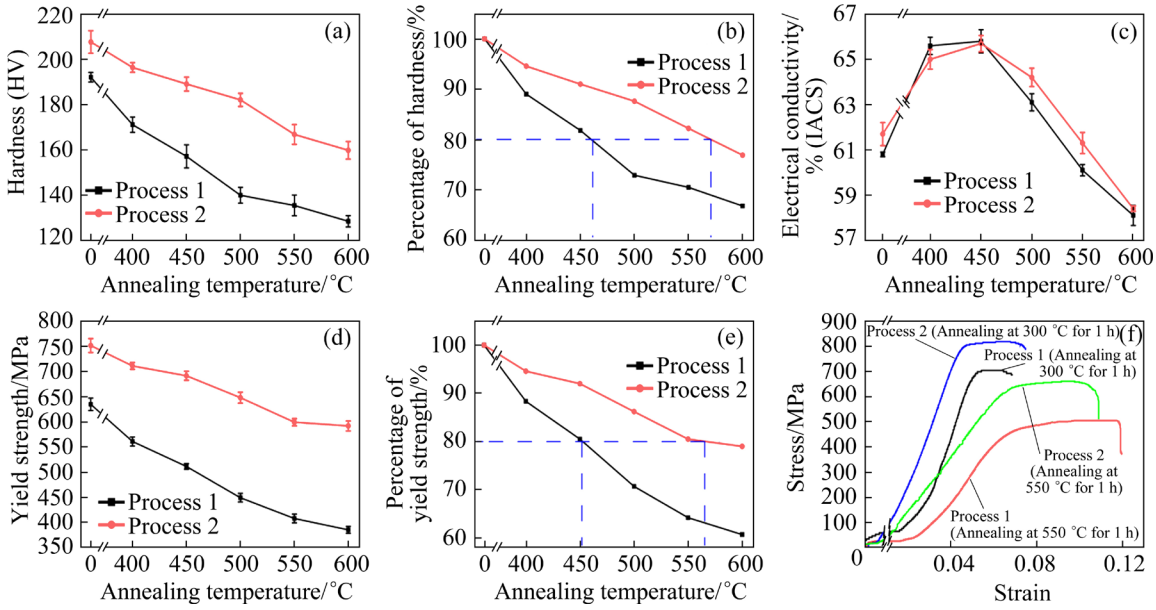

Fig. 15 Mechanical properties of Cu−6.5Fe−0.3Mg alloys after isochronous annealing for 1 h: (a) Vickers hardness; (b) Percentage of hardness; (c) Conductivity; (d) Yield strength; (e) Percentage of yield strength; (f) Engineering stress−strain curves

using Process 2 had greater softening resistance than that prepared using process 1. The softening temperatures of the Cu−6.5Fe−0.3Mg alloys prepared using Processes 1 and 2 were 460 and 570 °C, respectively. Furthermore, the percentage of yield strength in Fig. 15(e) follows the same trend as that in Fig. 15(b). Moreover, the conductivities of the alloys prepared using the two different processes initially increased and subsequently decreased as the annealing temperature increased, and did not differ significantly from each other. The peak conductivity was approximately 65.8% (IACS) (Fig. 15(c)).

Figure 16 shows the Vickers hardness values of the Cu−6.5Fe−0.3Mg alloys after isothermal annealing at 550 °C. The Vickers hardness values of the alloys prepared using the two processes decreased rapidly and reached equilibrium gradually over time. The Vickers hardness of the alloy prepared using Process 2 decreased more slowly than that prepared using Process 1. It took 46 min longer for the hardness of the alloy prepared using Process 2 to drop to 80% of the initial value than it took for the hardness of the alloy prepared using Process 1 to drop by the same amount. This demonstrates that the alloy prepared using Process 2 had greater softening resistance.

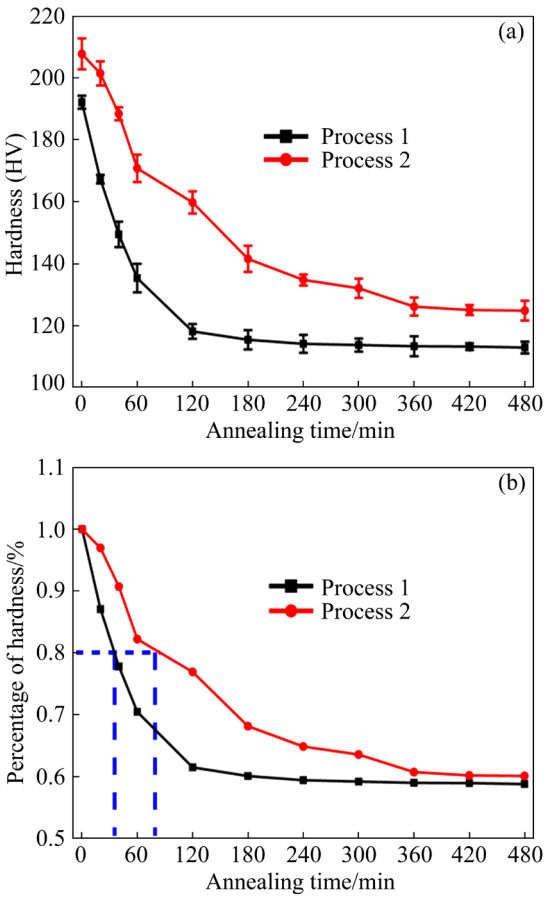

Fig. 16 Vickers hardness (a) and percentage of hardness (b) of Cu−6.5Fe−0.3Mg alloys after isothermal annealing at 550 °C

4 Discussion

4.1 Recrystallization theory

4.1.1 Recrystallization kinetics

After large plastic deformation, the alloys recovered and recrystallized successively during heat treatment. However, the mechanical properties of the alloys were greatly reduced in the recrystallization stage. The recrystallization volume fraction (X_V) is the standard used to measure the degree of recrystallization, which is closely related to the change in Vickers hardness with annealing time (Fig. 16), and can be expressed using the following formula [18,19]:

$$X_V=\frac{HV_I-HV_t}{HV_I-HV_{Rex}} \quad (1)$$

where HV_I is the Vickers hardness of the alloy after aging at 300 °C for 1 h, HV_t is the hardness after a given annealing time t, and HV_{Rex} is the hardness of fully recrystallized material. The volume fraction change of recrystallization during annealing at 550 °C was calculated, as shown in Fig. 17(a). It is obvious that the recrystallization volume fraction of the alloy prepared using Process 1 reached a peak faster than that of the alloy prepared using Process 2. The functional relationship between the volume fraction of alloy recrystallization and the annealing time can be described by the Johnson−Mehl−Avrami−Kolmogorov (JMAK) equation [18,19]:

$$X_V=1-\exp(-kt^n) \quad (2)$$

where k is a constant and n is the Avrami exponent, which reflect the nucleation and growth characteristics of the recrystallized grains, respectively. The recrystallization volume fraction expression of the alloys prepared using the two processes can be obtained from Fig. 17(b). The recrystallization volume fractions were calculated after annealing at 550 °C for 1 h, and the results are shown in Fig. 17(a). The results show that the calculated values were basically consistent with the measured values (Fig. 6). In addition, the values of the Avrami exponent were lower than the theoretical value of 3 (for recrystallization with

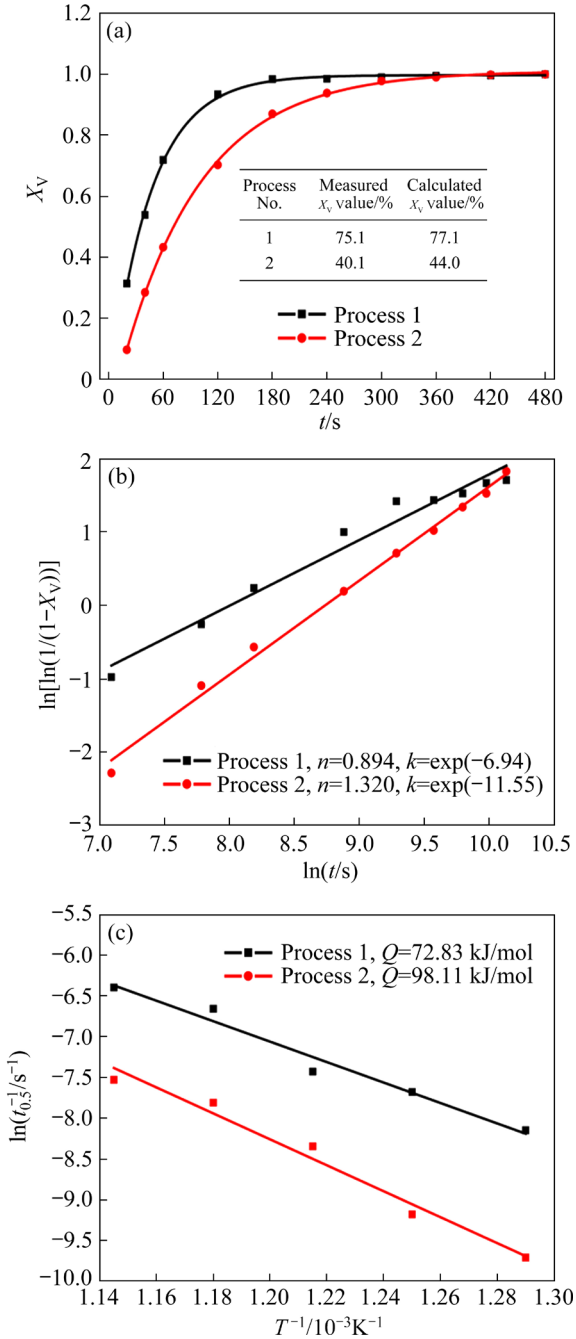

Fig. 17 Recrystallization kinetics curves of alloy: (a) Volume fraction of recrystallization; (b) Linear graph of ln[ln(1/(1−X_V))]−ln t; (c) Linear graph of ln $t_{0.5}^{-1}$ −T^{-1}

site-saturated nucleation), which indicates that the recrystallized grains of the alloy were formed by non-random nucleation [20].

In general, the recrystallization rate is commonly represented by the following classical Arrhenius equation [20]:

$$\frac{1}{t_{0.5}}=A\exp[-Q_R/(RT)] \quad (3)$$

where $t_{0.5}$ is the annealing time corresponding to a recrystallization ratio of 50%, Q_R is the recrystallization activation energy, A is a constant, R is the molar gas constant, and T is the thermodynamic temperature. The following formula can be obtained by simultaneously taking the logarithms of both sides of Eq. (3): $\ln t_{0.5}^{-1} = -Q_R/(RT)+\ln A$. The mathematical relationship between $\ln t_{0.5}^{-1}$ and T^{-1} is described in Fig. 17(c).

The Q value of the Cu−6.5Fe−0.3Mg alloy prepared using Process 2 was 98.11 kJ/mol, which was 25.28 kJ/mol higher than that of the alloy prepared using Process 1. This demonstrates that the recrystallization of the alloy prepared using Process 2 required a higher activation energy. In other words, recrystallization was less likely to occur.

4.1.2 Driving pressure for grain growth

The alloys prepared using the two processes demonstrated different resistances to the high temperature recrystallization (Figs. 4−6). The dislocations move and rearrange, and spontaneously combine to a low-energy state to form sub-crystals during high-temperature annealing [21]. The recrystallized grains formed by the consolidation of the sub-crystals grow through grain boundary migration and mutual engulfment. Therefore, the driving pressure for grain growth (P) after large plastic deformation depends mainly on dislocation density, which can be expressed using the following formula [22]:

$$P=KGb^2\rho_{Cu} \quad (4)$$

where K(=0.5) is a constant, G represents the shear modulus of the Cu matrix, and ρ_{Cu} represents the difference in the Cu matrix dislocation density before and after annealing. The related parameters are shown in Table 1. The dislocation density value can be obtained using Eqs. (5) and (6) [27,28]:

$$\rho=3.46\varepsilon/(Db) \quad (5)$$

$$\beta\cos\theta=K\lambda/D+(4\sin\theta)\varepsilon \quad (6)$$

where ε and D represent micro-strain and grain size, respectively, β and θ are the half-width and diffraction angle, respectively, and K(=0.9) and λ(=0.15405 nm) represent the material constant and the incident wavelength of XRD, respectively. The $\beta\cos\theta$−4$\sin\theta$ linear fitting relationship is obtained from the XRD data in Fig. 7. Therefore, the dislocation density can be obtained in conjunction

with Eq. (5). The driving pressure of grain growth indicates the tendency toward grain growth. The greater the driving force of grain growth is, the more easily the grain boundary migrates and the more easily the grain grows. According to Eqs. (4)−(6), the average P values of the Cu−6.5Fe−0.3Mg alloys prepared using Processes 1 and 2 were 1.36 and 1.32 MPa, respectively, during annealing at 550 °C. The calculated results show that the grain boundary of the alloy prepared using Process 1 migrated more readily and the grains were more readily coarsened than those of the alloy prepared using Process 2.

Table 1 Relevant parameters of model

Parameter	Value	Ref.
M	3.06	[23,24]
G_{Cu}/GPa	46	[23,24]
G_{Fe}/GPa	58	[23,24]
b	0.2556	[25]
v	0.34	[25]
α_{Cu}	0.26	[23]
α_{Fe}	0.3294	[23]
K_y/(MPa·m$^{1/2}$)	0.15	[26]

M is the Taylor factor; v is Poisson's ratio; α_{Cu} and α_{Fe} are the lattice constants of copper and iron, respectively; K_y is the Hall−Petch slope

The analysis of the recrystallization activation energy and driving pressure for grain growth showed that the Cu−6.5Fe−0.3Mg alloy prepared using Process 2 was better able to resist recrystallization and grain coarsening than the alloy prepared using Process 1.

4.2 Recrystallization mechanism

The Fe phases in the alloys prepared using the two processes were transformed into Fe fibers (Fig. 3 and Fig. 6), and numerous Fe phases were precipitated after thermomechanical treatment. Nano precipitates inhibit dislocation movement, grain boundary migration, and grain coarsening by pinning dislocations and grain boundaries [29]. Part of the driving pressure for grain growth by the curvature of the grain boundary is offset by the pinning pressure exerted by the particles at the grain boundary, and the Zener pinning pressure P_Z is expressed by the following formula [22]:

$$P_Z = 3f\gamma/(2r) \quad (7)$$

where f and r are the volume fraction and radius of the second phase, respectively, and γ is the boundary surface energy per unit area. It is obvious that the Zener pinning pressure is closely related to the ratio of the precipitate volume fraction to the precipitation radius. Mg can effectively promote the precipitation kinetics of the Fe phase and increase the density of the precipitates [17]. Furthermore, the Mg atoms distributed at the interface of the Cu/Fe phase can inhibit the coarsening of the Fe phase, which can increase the Zener pinning pressure of the precipitates relative to the grain boundary, thereby increasing the recrystallization temperature of the alloy. According to the data in Table 2, there was little difference between the ratios of the volume fractions and the radii of the precipitates of the alloys prepared using the two processes.

The analysis shows that there was little difference between the sizes and volume fractions of the precipitates in the alloys prepared using the two processes, and their effects on the dislocation Zener pinning pressure were basically the same. However, the density of the Fe fibers in the alloy prepared using Process 2 was higher than that of the alloy prepared using Process 1. This may be the main reason for the fact that the alloy prepared using Process 2 had greater recrystallization resistance.

A schematic diagram of the evolution of dislocation and grain morphology during heat treatment is shown in Fig. 18. The density of the Fe fibers in the Cu−6.5Fe−0.3Mg alloy prepared using Process 2 increased significantly (Fig. 18(b1)). As shown in Figs. 18(a2) and (b2), the Fe fibers formed a dense barrier that effectively inhibited the movement of dislocations and the migration of grain boundaries in the X direction (rolling direction), and reduced the mean free path of their movement. The barrier effectively inhibited the nucleation and growth of the recrystallized grains. However, when the heat treatment temperature was greater than 500 °C, the Fe fibers fractured and spheroidized [30,31], which greatly reduced their inhibitory effect on dislocation movement and recrystallization. In addition, the Mg atoms distributed around the Fe phase (Fig. 3) effectively enhanced the stability of the Fe fibers and slowed down their fracture and spheroidization. This was consistent with the previous findings [12].

Table 2 Calculated (σ_{Total}) and measured (σ) values of yield strength

Parameter	Alloy prepared by Process 1		Alloy prepared by Process 2	
	Aging at 300 °C	Annealing at 550 °C	Aging at 300 °C	Annealing at 550 °C
d_{precip}/nm	7.21	7.82	6.81	7.65
f_{precip}/%	0.37	0.358	0.348	0.354
d_G/μm	1.68	3.56	2.65	3.268
ρ_{Cu}/m^{-2}	9.87×10^{14}	7.78×10^{13}	1.72×10^{15}	8.41×10^{14}
ρ_{Fe}/m^{-2}	2.58×10^{14}	1.46×10^{14}	7.21×10^{14}	1.58×10^{14}
σ_0/MPa	60	60	60	60
$\Delta\sigma_{Orowan}$/MPa	158.6	145.7	158	147.2
$\Delta\sigma_{d\text{-}all}$/MPa	290.2	89.6	389	261.4
$\Delta\sigma_{GB}$/MPa	115	80	92.6	83
$\Delta\sigma_{SS}$/MPa	23	23	23	23
σ_{Total}/MPa	646.8	398	722.6	578.7
σ/MPa	635	407.7	752	599.3

d_{precip} is the precipitated phase diameter; f_{precip} is the precipitated phase volume fraction; d_G is the grain diameter; ρ_{Cu} is the dislocation density of the copper matrix; ρ_{Fe} is the dislocation density of the iron matrix; σ_0 is the strength of the Cu matrix; $\Delta\sigma_{Orowan}$ is precipitation strengthening; $\Delta\sigma_{d\text{-}all}$ is the dislocation strengthening; $\Delta\sigma_{GB}$ is the grain-boundary strengthening; $\Delta\sigma_{SS}$ is the solid solution strengthening; σ_{Total} is the calculated value of yield strength; σ is the actual measured value of yield strength

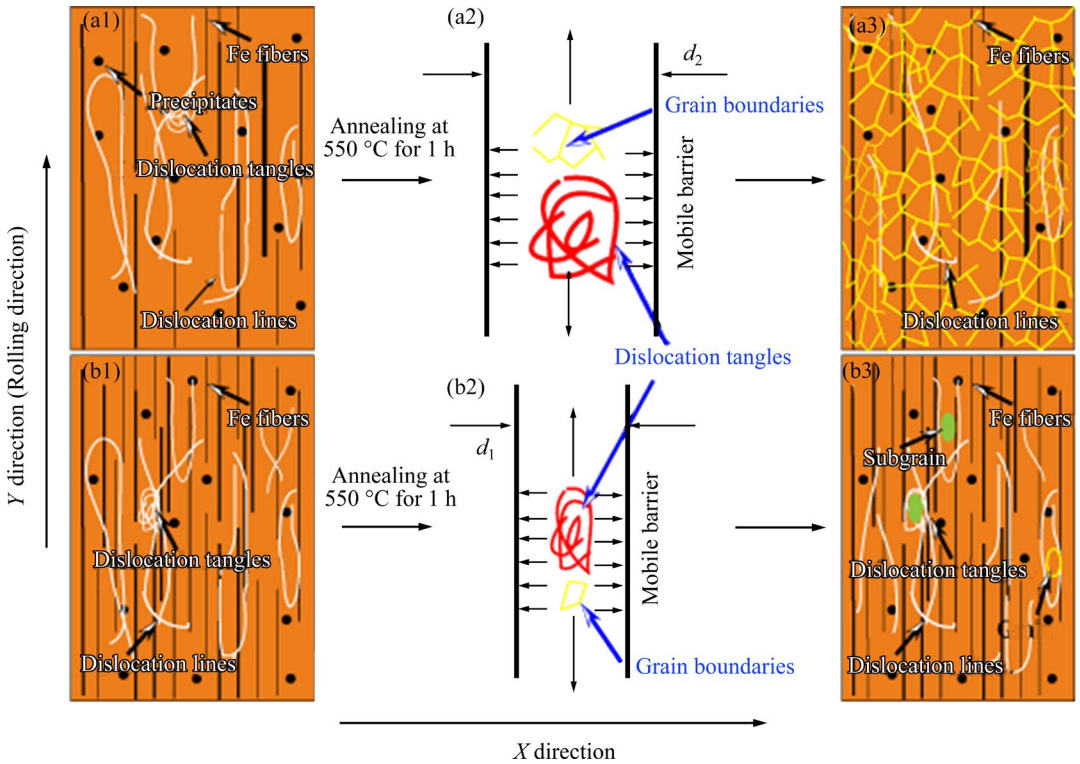

Fig. 18 Schematic diagram showings relationship between Fe fiber and dislocation (a1, a3, b1, b3), and Fe fibers inhibiting dislocation motion (d_1 and d_2 are Fe fiber spacings) (a2, b2): (a1−a3) Process 1; (b1−b3) Process 2

The alloy prepared using Process 2 had a higher recrystallization activation energy and a smaller driving pressure for grain growth than the alloy prepared using Process 1. This may be attributed to the fact that the dense Fe fibers inhibited dislocation movement and grain boundary migration. Therefore, the dense Fe fibers were the main reason for the stronger recrystallization

resistance of the Cu−6.5Fe−0.3Mg alloy prepared using Process 2.

4.3 Softening mechanism

During the annealing process, the softening temperature of the alloy prepared by Process 2 (570 °C) was much higher than that of the alloy prepared by Process 1 (460 °C) (Figs. 15 and 16). The yield strengthening of a Cu alloy is mainly determined by the joint action of dislocation strengthening, precipitation strengthening, grain boundary strengthening, and solution strengthening [32−34]. During the heat treatment, the dislocation density, precipitate density, and grain size changed, resulting in a change in the yield strength of the alloy. Therefore, the strengthening mechanism of the Cu−6.5Fe−0.3Mg alloys after aging at 300 °C and annealing at 550 °C was investigated to determine the softening behavior of the alloys during heat treatment.

(1) Dislocation strengthening ($\Delta\sigma_{\text{d-all}}$)

Dislocations are staggered and tangled by external forces, which hinder their movement [37]. Therefore, dislocation strengthening is one of the main methods by which Cu alloys are strengthened. The strengthening effect is closely related to the dislocation density (ρ) [28]. The matrix phases in Cu−Fe alloys are mainly Cu and Fe phases. Therefore, it is expected that the dislocation strengthening ($\Delta\sigma_{\text{d-all}}$) of the Cu−6.5Fe−0.3Mg alloy would result from the combined effect of the dislocations in the two phases, as expressed by the following equation [28]:

$$\sigma_{\text{d-all}} = w_{\text{Cu}}\sigma_{\text{dCu}} + w_{\text{Fe}}\sigma_{\text{dFe}} \quad (8)$$

where w_{Cu} and w_{Fe} represent the mass fractions of Cu and Fe, respectively, and σ_{dCu} and σ_{dFe} are the dislocation strengthening values in the Cu matrix and Fe phase, respectively.

(2) Precipitation strengthening ($\Delta\sigma_{\text{Orowan}}$)

Cu−Fe alloys are typical precipitation-strengthened alloys. When dislocations bypass the precipitated Fe phases, they hinder the movement of dislocations, thereby improving the stress resistance of the alloys. Its reinforcement model is combined with Orowan reinforcement [24−26].

(3) Grain-boundary strengthening ($\Delta\sigma_{\text{GB}}$)

Two crystal grains with different orientations undergo plastic deformation under the action of external force, and the dislocations inside the crystal grains slip along the crystal planes to form dislocation accumulations, thereby improving the yield strength of the alloy. Its reinforced model conforms to the Hall−Petch model [26].

(4) Solid-solution strengthening ($\Delta\sigma_{\text{SS}}$)

The Mg and Fe atoms dissolved in the Cu matrix cause lattice distortion, which increases the stress required for dislocation movement and the difficulty of dislocation slip [35]. At room temperature, the solid solubility of the Fe atoms in the Cu matrix is small and the addition of Mg promotes the precipitation of the Fe phase. Therefore, the solid solution strengthening effect caused by elemental Fe can be ignored.

Equation (9) can be used to calculate the total yield strength of an alloy [36]:

$$\Delta\sigma_{\text{Total}}=\Delta\sigma_0+\Delta\sigma_{\text{Orowan}}+\Delta\sigma_{\text{d-all}}+\Delta\sigma_{\text{GB}}+\Delta\sigma_{\text{SS}} \quad (9)$$

where σ_0 is the strength of the Cu matrix (generally 60 MPa).

The values of the related parameters are shown in Table 1. Table 2 lists the contribution of each strengthening mechanism to the total yield strength.

The calculated yield strengths of the aged Cu−6.5Fe−0.3Mg alloys prepared by Process 1 and Process 2 are 646.8 and 722.6 MPa respectively; they are 398.3 and 578.7 MPa after annealing at 550 °C for 1 h, which are consistent with the experimental results. It is worth noting that the dislocation strengthening of the alloy prepared by Process 2 always dominates before and after annealing at 550 °C for 1 h, while the dominant strengthening mechanism of the alloy prepared by Process 1 changes from dislocation strengthening to precipitation strengthening. The precipitation strengthening, grain boundary strengthening and solution strengthening of the alloys prepared by two processes have no significant changes before and after annealing at 550 °C for 1 h. It is obvious that the loss of alloy strength (the softening mechanism) is mainly attributable to the decrease in dislocation strengthening after annealing. The dislocation strengthening loss rate of the alloy prepared using Process 2 (32.8%) was far lower than that of the alloy prepared using Process 1 (69.1%). This is mainly attributable to the fact that the dense Fe fibers in the Cu−6.5Fe−0.3Mg alloy prepared using Process 2 inhibited the movement and annihilation of dislocations, resulting in higher softening temperature of the alloy.

5 Conclusions

(1) The recrystallization activation energy and driving pressure of the grain growth of the alloy prepared using Process 2 were 98.11 kJ/mol and 1.32 MPa, respectively. Therefore, the Q value was 25.28 kJ/mol higher and the P value was 0.04 MPa lower than those of the alloy prepared using Process 1. The Cu−6.5Fe−0.3Mg alloy prepared using Process 2 was better able to resist recrystallization and grain coarsening than the alloy prepared using Process 1.

(2) The softening mechanism of Cu−6.5Fe−0.3Mg alloys prepared using the two processes was mainly attributable to the synergistic effects of precipitation strengthening, grain boundary strengthening, and dislocation strengthening; the loss of dislocation strengthening was the main factor. The density of Fe fibers in the Cu−6.5Fe−0.3Mg alloy prepared using Process 2 was higher than that of the alloy prepared using Process 1. The dense Fe fibers effectively inhibited the annihilation of dislocations and the migration of grain boundaries, resulting in the higher softening temperature of the alloy prepared by Process 2.

(3) The softening temperature, Vickers hardness, yield strength, and tensile strength of the alloy prepared using Process 2 were 570 °C, HV 207.7, 752 MPa, and 818 MPa, respectively, and after aging at 300 °C for 1 h, they were 110 °C, HV 15, 117 MPa, and 114 MPa higher, respectively, than those of the alloy prepared using Process 1. The peak conductivities of the alloys prepared using the two processes were not significantly different, i.e., approximately 65.8% (IACS).

CRediT authorship contribution statement

Zhen-xia LIU: Data curation, Investigation, Formal analysis; **Da-wei YUAN:** Conceptualization, Methodology, Writing − Original draft preparation; **Xin LUO:** Writing − Reviewing; **Lan-hao WANG:** Data analysis; **Jin-shui CHEN:** Investigation, Formal analysis; **Hui-ming CHEN:** Formal analysis; **Xiang-peng XIAO:** Conceptualization, Writing − Reviewing & editing; **Bin YANG:** Supervision and editing.

Declaration of competing interest

The authors declare that they have no known competing financial interests or personal relationships that could have appeared to influence the work reported in this paper.

Acknowledgments

The authors are pleased to acknowledge the financial supports from the Department of Science and Technology and other Provincial and Ministerial Level Projects, China (No. 204306800086), Science and Technology Projects of Ganzhou Science and Technology Bureau, China (No. 204301000194), and the Science and Technology Project of Jiangxi Provincial Department of Education, China (No. 204201400853).

References

[1] LI Yong, YI Dan-qing, ZHANG Jian-bo. Comparative study of the influence of Ag on the microstructure and mechanical properties of Cu−10Fe in situ composites [J]. Journal of Alloys and Compounds, 2015, 647: 413−418. http://dx.doi.org/10.1016/j.jallcom.2015.05.252.

[2] SUN Xiao-jun, HE Jie, CHEN Bin, ZHANG Li-li, JIANG Hong-xiang, ZHAO Jiu-zhao, HAO Hong-ri. Microstructure formation and electrical resistivity behavior of rapidly solidified Cu−Fe−Zr immiscible alloys [J]. Journal of Materials Science & Technology, 2020, 44: 201−208. http://dx.doi.org/10.1007/s11661-010-0432-y.

[3] LIU Shi-chao, JIE Jin-chuan, GUO Zhong-kai, YUE Shi-peng, LI Ting-ju. A comprehensive investigation on microstructure and magnetic properties of immiscible Cu−Fe alloys with variation of Fe content [J]. Materials Chemistry and Physics, 2019, 238: 1−9. https://doi.org/10.1016/j.matchemphys.2019.121909.

[4] GAO Hai-yan, WANG Jun, SUN Bao-de. Effect of Ag on the thermal stability of deformation processed Cu−Fe in situ composites [J]. Journal of Alloys and Compounds, 2009, 469(1/2): 580−586. https://doi.org/10.1016/j.jallcom.2008.02.013.

[5] WANG Meng, JIANG Yan-bin, LI Zhou, XIAO Zhu, GONG Shen, QIU Wen-ting, LEI Qian. Microstructure evolution and deformation behaviour of Cu−10wt.%Fe alloy during cold rolling [J]. Materials Science and Engineering A, 2021, 801(9): 140379. https://doi.org/10.1016/j.msea.2020.140379.

[6] ZOU Jin, LU De-ping, FU Qing-feng, LIU Ke-ming, JIANG Jiang. Microstructure and properties of Cu−Fe deformation processed in-situ composite [J]. Vacuum, 2019, 167: 54−58. https://doi.org/10.1016/j.vacuum.2019.05.030.

[7] GUO J Q, YANG H, LIU P, JIA S G, HUANG H, Microstructure evolution and performance of Cu−10Fe−2Ag−0.15Zr in situ composite by cold rolling [J]. Materials Research Innovations, 2011, 15: 404−407. https://doi.org/10.1179/143307511X12858957675237.

[8] LIU Ke-ming, HUANG Zhi-kai, ZHANG Xing-wang, LU De-ping, ATRENS A, ZHOU Hai-tao, YIN Yi, YU Jiu-ming, GUO Wei. Influence of Ag micro-alloying on the thermal stability and ageing characteristics of a Cu−14Fe in-situ

composite [J]. Materials Science and Engineering A, 2016, 673: 1−7. https://doi.org/10.1016/j.msea.2016.07.017.

[9] YUAN Da-wei, CHEN Jin-shui, XIAO Xiang-peng, HAN Bao-jun, HUANG Hao, LIU Bai-xiong, YANG Bin. Microstructure and properties of Cu−Fe−Cr−Ag alloy prepared by directional solidification and upward continuous casting [J]. Metallurgical and Materials Transactions A: Physical Metallurgy and Materials Science, 2021, 52: 2489−2500. https://doi.org/10.1007/s11661-021-06239-z

[10] HONG S I, SONG J S. Strength and conductivity of Cu−9Fe−1.2X (X=Ag or Cr) filamentary microcomposite wires [J]. Metallurgical and Materials Transactions A: Physical Metallurgy and Materials Science, 2001, 32(4): 985−991. https://doi.org/10.1007/s11661-001-0356-7.

[11] SUN Yu-qing, PENG Li-jun, HUANG Guo-jie, XIE Hao-feng, MI Xu-jun, LIU Xin-hua. Effects of Mg addition on the microstructure and softening resistance of Cu−Cr alloys [J]. Materials Science and Engineering A, 2020, 776: 139009. https://doi.org/10.1016/j.msea.2020.139009.

[12] YUAN Da-wei, XIAO Xiang-peng, LUO Xin, WANG Hang, HAN Bao-jun, LIU Bai-xiong, YANG Bin. Effect of multi-stage thermomechanical treatment on Fe phase evolution and properties of Cu−6.5Fe−0.3Mg alloy [J]. Materials Characterization, 2022, 185: 111707. https://doi.org/10.1016/j.matchar.2021.111707.

[13] GUO Jun-qing, YANG He, LIU Ping, JIA Shu-guo, BI Li-ming. Effect of Zr on thermal stability of Cu−Fe in situ composite [J]. Advances Materials Research, 2011, 150/151: 1462−1465. https://doi:10.4028/www.scientific.net/AMR.150-151.1462.

[14] XIA Cheng-dong, ZHANG Wan, KANG Zhan-yuan, JIA Yan-lin, WU Yi-feng, ZHANG Rui, XU Gen-ying, WANG Ming-pu. High strength and high electrical conductivity Cu−Cr system alloys manufactured by hot rolling–quenching process and thermomechanical treatments [J]. Materials Science and Engineering A, 2012, 538: 295−301. https://doi.org/10.1016/j.msea.2012.01.047.

[15] SARKAR S, SRIVASTAVA C, CHATTOPADHYAY K. Development of a new class of high strength copper alloy using immiscibility route in Cu−Fe−Si system: Evolution of hierarchical multi-scale microstructure [J]. Materials Science and Engineering A, 2018, 723: 38−47. https://doi.org/10.1016/j.msea.2018.03.026.

[16] ZHANG Ping, LEI Qian, YUAN Xiao-bo, SHENG Xiao-fei, JIANG Dong, LI Yun-ping, LI Zhou. Microstructure and mechanical properties of a Cu−Fe−Nb alloy with a high product of the strength times the elongation [J]. Materials Today Communications, 2020, 25(11): 101353. https://doi.org/10.1016/j.mtcomm.2020.101353.

[17] YUAN Da-wei, ZENG Hao, XIAO Xiang-peng, WANG Hang, HAN Bao-jun, YANG Bin. Effect of Mg addition on Fe phase morphology, distribution and aging kinetics of Cu−6.5Fe alloy [J]. Materials Science and Engineering A, 2021, 812: 141064. https://doi.org/10.1016/j.msea.2021.141064.

[18] ZHU K Y, CHAUBET D, BACROIX B, BRISSET F. A study of recovery and primary recrystallization mechanisms in a Zr−2Hf alloy [J]. Acta Materialia, 2005, 53: 5131−5140. https://doi.org/10.1016/j.actamat.2005.07.034.

[19] YU Fang-xin, CHENG Jian-yi, SHEN Bin. Precipitation sequence of Cu−Cr−Zr−Mg alloy during early aging stage [J]. Materials Characterization, 2013, 81: 68−75. http://dx.doi.org/10.1016/j.matchar.2013.04.008.

[20] LUO Ze-yu, LUO Fu-xin, XIE Wei-bin, CHEN Hui-ming, WANG Hang, YANG Bin. A study on annealing-induced softening in cold drawn Cu−Cr−Sn alloy [J]. Materialwissenschaft and Werkstofftechnik, 2018, 49: 1325−1334. https://doi.org/10.1002/mawe.201700201.

[21] ZENG Hao, SUI Han, WU Shang-jiang, LIU Jin-ping, WANG Hang, ZHANG Jian-bo, YANG Bin. Evolution of the microstructure and properties of a Cu−Cr−(Mg) alloy upon thermomechanical treatment [J]. Journal of Alloys and Compounds, 2020, 857: 157582. https://doi.org/10.1016/j.jallcom.2020.157582.

[22] MOROZOVA A, BELYAKOV B, KAIBYSHEV C. Effect of annealing treatment on ECAP structure in Cu−Cr−Zr bronze [C]//AIP Conference Proceedings. Tomsk, Russia, 2017: 1−4. https:// doi.org/10.1063/1.5013823.

[23] XIE Ming-wang, HUANG Wei, CHEN Hui-ming, GONG Liu-kui, XIE Wei-bin, WANG Hang, YANG Bin. Microstructural evolution and strengthening mechanisms in cold-rolled Cu−Ag alloys [J]. Journal of Alloys and Compounds, 2021, 851:156893. https://doi.org/10.1016/j.jallcom.2020.156893.

[24] WANG Meng, ZHANG Rui, XIAO Zhu, GONG Shen, JIANG Yan-bin, LI Zhou. Microstructure and properties of Cu−10wt.%Fe alloy produced by double melt mixed casting and multi-stage thermomechanical treatment [J]. Journal of Alloys and Compounds, 2020, 820: 1−10. https://doi.org/10.1016/j.jallcom.2019.153323.

[25] OROWAN E. Fracture and strength of solids [J]. Reports on Progress in Physics, 1949, 12: 185−232. http://dx.doi.org/10.1088/0034-4885/12/1/309.

[26] PENG Li-jun, XIE Hao-feng, HUANG Guo-jie, XU Gao-lei, YIN Xiang-qian, FENG Xue, MI Xu-jun, YANG Zhen. The phase transformation and strengthening of a Cu−0.71wt.% Cr alloy [J]. Journal of Alloys and Compounds, 2017, 708: 1096−1102. http://dx.doi.org/10.1016/j.jallcom.2017.03.069.

[27] ZHAO Y H, LIAO X Z, JIN Z, VALIEV R Z, ZHU Y T. Microstructures and mechanical properties of ultrafine grained 7075 Al alloy processed by ECAP and their evolutions during annealing [J]. Acta Materialia, 2004, 52(15): 4589−4599. https://doi.org/10.1016/j.actamat.2004.06.017.

[28] CHENG H, WANG H Y, XIE Y C, TANG Q H, DAI P Q. Controllable fabrication of a carbide-containing FeCoCrNiMn high-entropy alloy: Microstructure and mechanical properties [J]. Materials Science and Technology, 2017, 33(17): 2032−2039. https://doi.org/10.1080/02670836.2017.1342367.

[29] LI Jia-zhi, DING Hua, LI Bao-mian, GAO Wei-lin, BAI Jie, SHA Gang. Effect of Cr and Sn additions on microstructure, mechanical−electrical properties and softening resistance of Cu−Cr−Sn alloy [J]. Materials Science and Engineering A, 2021, 802(1): 140628. https://doi.org/10.1016/j.msea.2020.140628.

[30] GAO Hai-yan, WANG Jun, SHU Da, SUN Bao-de.

Microstructure and properties of Cu−11Fe−6Ag in situ composite after thermo-mechanical treatments [J]. Journal of Alloys and Compounds, 2007, 438(1/2): 268−273. https://doi.org/10.1016/j.jallcom.2006.08.027.

[31] GAO Hai-yan, WANG Jun, SHU Da, SUN Bao-de. Effect of Ag on the aging characteristics of Cu−Fe in situ composites [J]. Scripta Materialia, 2006, 54(11): 1931−1935. https://doi.org/10.1016/j.scriptamat.2006.02.006.

[32] GUO Xiao-li, XIAO Zhu, QIU Wen-ting, LI Zhou, ZHAO Zi-qian, WANG Xu, JIANG Yan-bin. Microstructure and properties of Cu−Cr−Nb alloy with high strength, high electrical conductivity and good softening resistance performance at elevated temperature [J]. Materials Science and Engineering A, 2019, 749: 281−290. http://dx.doi.org/10.1016/j.msea.2019.02.036.

[33] CHEN Jin-shui, WANG Jun-feng, XIAO Xiang-peng, WANG Hang, CHEN Hui-ming, YANG Bin. Contribution of Zr to strength and grain refinement in Cu−Cr−Zr alloy [J]. Materials Science and Engineering A, 2019, 756: 464−473. https://doi.org/10.1016/j.msea.2019.04.053.

[34] WANG Yu-jian, QU Jian-ping, WANG Xian-long, JIE Jin-chuan, LI Ting-ju. Effects of Y addition on the microstructure, properties and softening resistance of Cu−Cr alloy [J]. Journal of Alloys and Compounds, 2022, 902: 163816. http://dx.doi.org/10.1016/j.jallcom.2022.163816.

[35] HE J Y, WANG H, HUANG H L, XU X D, CHEN M W, WU Y, LIU X J, NIEH T G, AN K, LU Z P. A precipitation-hardened high-entropy alloy with outstanding tensile properties [J]. Acta Materialia, 2016, 102: 187−196. https://doi.org/10.1016/j.actamat.2015.08.076.

[36] MA Ka-ka, WEN Hai-ming, HU Tao, TOPPING T D, ISHEIM D, SEIDMAN D N, LAVERNIA E J, SCHOENUNG J M. Mechanical behavior and strengthening mechanisms in ultrafine grain precipitation-strengthened aluminum alloy [J]. Acta Materialia, 2014, 62: 141−155. http://dx.doi.org/10.1016/j. actamat.2013.09.042.

形变热处理对 Cu−6.5Fe−0.3Mg 合金再结晶和抗软化性能的影响

刘珍霞[1]，袁大伟[1]，罗 鑫[2]，王兰浩[2]，陈金水[2]，陈辉明[1]，肖翔鹏[1]，杨 斌[2]

1. 江西理工大学 先进铜产业学院，鹰潭 335000；
2. 江西理工大学 材料冶金化学学部，赣州 341000

摘 要：采用维氏硬度试验、拉伸试验、扫描电子显微镜和透射电子显微镜研究由工艺 1(冷轧热处理)和工艺 2(热/冷轧热处理)制备的 Cu−6.5Fe−0.3Mg(质量分数，%)合金的再结晶和抗软化性能。300 ℃时效后，采用工艺 2 制备的合金的软化温度、硬度和抗拉强度和比采用工艺 1 制备的合金分别增加了 110 ℃、HV 15 和 114 MPa。采用工艺 1 和工艺 2 制备的合金的再结晶活化能分别为 72.83 和 98.11 kJ/mol，且两种合金中析出相对晶界和位错的钉扎作用基本相同。软化机制主要归因于位错强化的损失。较高的 Fe 纤维密度抑制了位错的平均自由行程和晶界迁移，这是工艺 2 制备合金的软化温度更高的主要原因。

关键词：Cu−6.5Fe−0.3Mg 合金；热轧；再结晶活化能；软化机理；位错强化

(Edited by Wei-ping CHEN)